Scientia Iranica, Vol. 10, No. 1, pp 122–130
© Sharif University of Technology, January 2003

SCIENTIA
IRANICA

Research Note

Hydrodynamics of Two-Dimensional Laminar Turbid Density Currents

B. Firoozabadi*, B. Farhanieh[1] and M. Rad[1]

In this paper, the motion of turbid density currents, laden with fine solid particles, released on sloping beds and under still bodies of clear water, has been numerically investigated. The equations of mass, momentum and diffusion for unsteady, laminar flow are solved at the same time, in the fixed Cartesian directions, on a non-staggered grid using a finite volume scheme. The velocity-pressure coupling is handled by using the SIMPLEC method. Turbidity currents with uniform velocity and concentration enter the channel via a sluice gate into a lighter ambient fluid and move forward down-slope. At the front of this flow, a vortex forms and grows while moving downstream. Comparison of the computed height of the turbidity current with the experimental data shows a good agreement. In this paper, the deposition of particles and the effects of their fall velocity on concentration distribution are also investigated. The results show that the coarse particles settle rapidly and create maximum concentration on the bed. However, medium size particles of 50 microns, encountered during deposition, with a vertical velocity component due to up-lift flow, form a spongy layer near the bed. This layer, which could also be seen in experiments, shows the interaction of particles and the velocity components of fluid, especially near the bed. Fine particles of around and less than 10 microns are distributed in the main parts of the fluid concentration profiles, which are similar to that of salt-water density currents. Also, in this work, the structures of two grain sizes in the flow are investigated and the results show that fine particles, with the highest share of concentration in the main body of the flow, have the most effect in the total concentration distributions. However, the presence of coarse particles could affect the solid accumulation near the bed.

INTRODUCTION

Turbid water, moving from rivers into reservoirs, often goes below the strata of clear water and produces a phenomenon known as "turbid density current". These currents are quite different from free jet flow and river sediment transportation. Such flows are only produced due to the vertical density gradient. In fact, the magnitude of the driving force and corresponding velocity is directly proportional to the density gradient. A definition sketch of a turbidity current is presented in Figure 1.

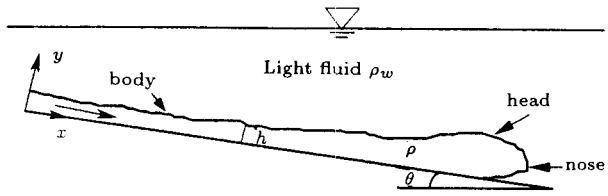

Figure 1. Definition sketch.

Density currents can be seen in the atmosphere during thunderstorms, dust storms in the desert, powder-snow avalanches in the mountains [1], movement of lava from erupting volcanoes [2] and gas movements through a mine [3].

In oceans, turbidity currents set up deposit and sedimentation movement on the seabed. The existence of living organisms and aeration deep in the ocean and near the ocean bed is a phenomenon caused by this current. The depositing of sediment on the ocean bed is a clear sign of the passage of turbidity currents. Determining the velocities of these currents can greatly improve understanding of the formation processes of undersea channels. The speed of turbidity currents,

*. *Corresponding Author, Department of Mechanical Engineering, Sharif University of Technology, P.O. Box 11365-8639, Tehran, I.R. Iran.*

1. *Department of Mechanical Engineering, Sharif University of Technology, P.O. Box 11365-8639, Tehran, I.R. Iran.*

known to break undersea cables [4], are estimated to be around 350 nautical miles per hour. Application of these current is important to various fields such as: The protection of sea faring vessels, atmospheric pollution, entomology and pest control, gas compression technology, meteorology and weather forecast, cleaning of oil spills, etc.

Turbidity current control is one of the known methods used for sedimentation control in reservoirs. The venting of the turbidity currents through bottom outlets to reduce the siltation of the reservoirs, has become common practice in many countries [5]. Understanding of the flow pattern and hydrodynamics of these currents would be a great help in increasing the useful life expectancy of a reservoir and in improving the quality of service water. Due to the high costs and the problems involved in obtaining field measurements of turbidity currents, there is not much field data available. Thus, much of the physical behavior of these phenomena is unknown. Chikita and Okumora [5] have measured the characteristics of the particle-laden inflows of the Katsurasawa reservoir in Hokkido, Japan. The results show that twelve hours after the flooding, due to melting snow, the turbulent turbidity currents, Reynolds and densimetric Froude numbers, lie between $7.1*10^4 - 5.8*10^5$ and $1.5 - 4.4$, respectively. These measurements, conducted at a depth of 165 m from the water surface, indicate that at the interface of clear water and turbidity current, entrainment occurred and resulted in a decrease in the temperature of the current. In fact, in addition to density differences due to the presence of particles, temperature differences may also add to the overall density gradients and thereby further complicating the nature of the currents. Ford and Johnson [6] also measured the mud-laden flow into the DeGgray reservoir, built on the Caddo River. Their results indicate that after the flooding, turbidity current flow rate jumped from 1.4 m^3/s to 700 m^3/s. Such an upsurge inflow rate can inevitably lead to bed erosion and, consequently, the deposition of the reservoir bed could be greatly washed away if the bottom outlet gates of the dam are opened. Turbidity currents in reservoirs under still bodies of clear water are characterized by a distinctive raised head, which is commonly referred to as a "front part", followed by a quasi-uniform flow regime called a "body part". The height of the head has been reported as being twice the body height [7]. For a density current flowing down a sloped bed, the size of the head continually increases. The current usually has a "nose" or foremost point raised a short distance above the bed. In these currents, the particles settle down, resulting in reduction of the density difference. On the other hand, the presence of a shear layer at the interface, due to the existence of two different fluids and, subsequently, the production of shear stresses, contribute to the formation of a large number of vortices, causing the entrainment of the upper lighter fluid into the turbidity current. Thus, the analysis of the flow characteristics becomes more complicated.

Von-Karmen was the first to analyze the dynamics of a density currents head, using Bernoulli equation, which was improved later by Benjamin [8]. Turner [7] has analyzed a one-dimensional density current for laminar and turbulent flows. Numerical investigations of density current for different modes and particle-laden flows have been undertaken by Akiyama and Stefan [9]. The authors assumed jet velocity distribution in a turbulent model and solved the equations of the turbidity current. Assuming the thickness of the deposit to be 5% of the current depth, Akiyama performed an integration of equations from the bed up to the interface. Using this method, knowing the boundary condition at the bed and assuming several variables at the interface, Akiyama managed to compute the depth, buoyancy flux, Richardson number and the non-dimensional average velocity in the flow direction. The results have been compared with the empirical results and show that the overall Richardson number, a short distance from the channel inlet, reaches a constant value. Differential solutions of the equations of the density current have been performed for special cases. Bonnecaze et al. [10] have solved the particle-laden density current equations as shallow water equations for unsteady, one-dimensional, uniform velocity and concentration on the flat plate. In the solution of equations, assumptions, such as no entrainment and the negligibility of viscosity, have been made. Bonnecaze solved the equations using the two-step Lax-Wendroff scheme [10]. The resulting solution is consistent with empirical results in terms of the shape and appearance of the particles density current front. Parker et al. [11] have combined the three equations of mass and momentum conservation with the inflow equation of the bed matter and solved them numerically. Stacey and Bowen [12] solved the equations of turbidity current for unsteady turbulent and one-dimensional cases, by neglecting the inertial terms and, thereby, obtaining the effects of particle fall velocity in the distribution of the flow velocity, concentration and depth of the current. Density current head has not been simulated in two-dimension. For example: Fukushima [13] has considered it as a semi-sphere and solved the equation in one-dimension. This paper presents the solution of the governing equations of turbid density currents for unsteady, two-dimensional and laminar flow, without any special assumptions for simplification of equations. The obtained results, especially of the shape and hydrodynamics of the front part of the turbidity currents, are compared with the experimental data and have reasonable agreement.

GOVERNING EQUATIONS

In solving the two-dimensional equations, the depth of the lighter fluid, H, is assumed remarkable compared to that of the turbidity current height, h. Due to the low concentration of the particles, the fluid could be assumed as Newtonian. Using Bousinesq approximation, the equations which describe the motion of a turbidity current, when the interaction of grains is unimportant and the suspension can be characterized by a single grain size (the case where two grain sizes are in suspension will be described later), can be expressed as:

$$\frac{\partial u}{\partial x} + \frac{\partial \nu}{\partial y} = 0, \tag{1}$$

$$\frac{\partial u}{\partial t} + u\frac{\partial u}{\partial x} + v\frac{\partial u}{\partial y} = -(1/\rho)\frac{\partial p}{\partial x} + g' \sin\theta + \nu\nabla^2 u, \tag{2}$$

$$\frac{\partial \nu}{\partial t} + u\frac{\partial \nu}{\partial x} + v\frac{\partial \nu}{\partial y} = -(1/\rho)\frac{\partial p}{\partial y} - g' \cos\theta + \nu\nabla^2 \nu, \tag{3}$$

$$\frac{\partial C}{\partial t} + u\frac{\partial C}{\partial x} + v\frac{\partial C}{\partial y} = v_f \frac{\partial C}{\partial y} \cos\theta + \lambda\nabla^2 C. \tag{4}$$

These equations are continuity, momentum and diffusion, respectively. The u and v are components of the velocity in x and y directions; C is the concentration of fluid and ρ is the density of the mixture. g' is the reduced acceleration of gravity and θ is the slope of the bed. C and g' are defined as follows:

$$C = (\rho - \rho_w)/(\rho_s - \rho_w),$$

$$g' = g(\rho - \rho_w)/\rho_w.$$

ν and λ are the viscosity and diffusivity of the fluid, respectively. The particles in the current are assumed dilute and non-cohesive with equal settling velocities. The pressure term, P, is defined as:

$$p = p_0 + \rho_w g H + \rho g(h - y). \tag{5}$$

p_0 is the free surface pressure and ρ_w is the density of clear water. Due to the formation of a shear layer and vortices at the interface of the current with the surrounding fluid, entrainment occurs which, in addition to the creation of the density gradient, also causes the increase of density current depth. The appearance of the pressure term in these equations is due to the variation of density and depth of current; hence, its gradient cannot be omitted, even in the presence of a free surface. The settling velocity of particles, ν_f, can be calculated from empirical relations such as Dietrich's [9]:

$$\nu_f = (\sigma\ g\ \nu\ w^*)^{1/3}, \tag{6}$$

$$\log w^* = -3.7617 + 1.92944(\log D^*) - 0.09815(\log D^*)^2 - 0.000575(\log D^*)^3 + 0.00056(\log D^*)^4,$$

$$D^* = \sigma g(d_s^3/\nu),$$

$$\sigma = (\rho_s - \rho_w)/\rho.$$

In the case of a current laden with two particle sizes, instead of Equation 4, the following equations are coupled with the momentum Equations 2 and 3.

$$\frac{\partial C_1}{\partial t} + u\frac{\partial C_1}{\partial x} + \nu\frac{\partial C_1}{\partial y} = \nu_{f1}\frac{\partial C_1}{\partial x} \cos\theta + \lambda\nabla^2 C_1, \tag{7}$$

$$\frac{\partial C_2}{\partial t} + u\frac{\partial C_2}{\partial x} + \nu\frac{\partial C_2}{\partial y} = \nu_{f2}\frac{\partial C_2}{\partial x} \cos\theta + \lambda\nabla^2 C_2, \tag{8}$$

In this case, the total concentration is $C = C_1 + C_2$. Indices 1 and 2 denote the particle sizes.

BOUNDARY CONDITIONS

The boundary conditions at the inlet are known. Similar to the experimental models, the caolinit-laden flow with uniform velocity and concentration enters the channel under the still bodies of water via a sluice gate, onto a surface inclined at angle θ. At the outflow-boundary, the streamwise gradients of all variables are set to zero. It is expected that modeling of the outlet has only a local effect on the flow field [14]. At the free surface, the rigid-lid approximation is made, then, the symmetry condition is applied that includes zero gradients and zero fluxes perpendicular to the boundary [14]. At the rigid walls, due to the no slip conditions and a pure depositing assumption, velocities and concentration gradients are set at zero. For the concentration equation, zero gradient conditions normal to the vertical walls and zero-flux conditions normal to the bottom are applied.

SOLUTION PROCEDURE

The governing equations are solved by a finite-volume method using boundary fitted coordinates. The continuity, momentum and diffusion equations are solved for the velocity components and concentration u, v and C in the fixed Cartesian directions on a non-staggered grid. All the variables are, thus, stored at the center of the control volume. The velocity components at the control volume faces are computed by the Rhie-Chow interpolation method [15] and the

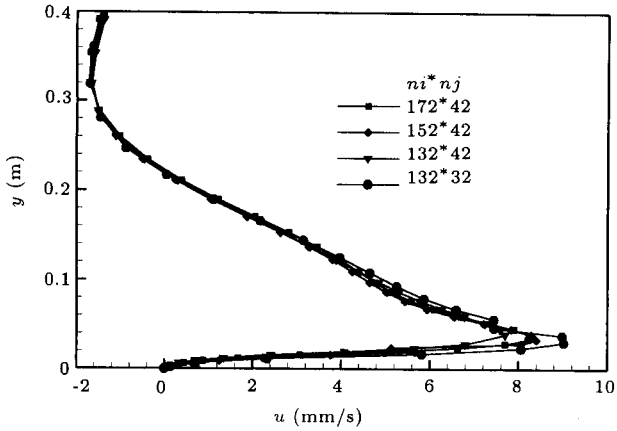

Figure 2. The effect of mesh size on the velocity distribution of recirculating zone.

pressure-velocity coupling is handled by the SIMPLEC method. The convective terms are treated by the hybrid scheme. TDMA-based algorithms are applied for solving the algebraic equations. Further details are provided by Davidson and Farhanieh [16]. The solution procedure is iterative and the computations are terminated when the sums of absolute residuals normalized by the inflow fluxes are below 10^{-4} for all variables. To achieve convergence in the solutions, under-relaxation factors of 0.5 were chosen for all the variables. At the initial time step, depending on velocity and slope, around 3000-5000 iterations are required to achieve convergence in the velocity fields. However, for the concentration field, convergence is much quicker. Due to the progression of the flow front, mesh points are chosen as uniform in the flow direction but, in the normal direction, the grid points are distributed in a non-uniform manner with a higher concentration of grids close to the bed surface. Each control volume contains one node at its center, but the boundary adjacent volumes contain two nodes. The effect of different mesh size on flow progression and the velocity profiles at the center of the recirculation zone of the head were obtained. The results are presented in Figure 2. As seen from this figure, no changes in the results can be observed by increasing the mesh size to greater than 172*42. Thus, the mesh size of 152*42 was chosen to perform the computations.

RESULTS AND DISCUSSION

The contour lines of concentration for a current containing 50-micron particles and after 500 sec of forward movement, are presented in Figure 3. The shape of the flow front and velocity vectors is visible in the figure. It can be seen that the recirculation created at the flow front, its greater depth and front shape, is due to the velocity distribution at the front. For this reason, the front depth is approximately two times as large as the body depth behind it. This is consistent with the laboratory results obtained by Turner [7] and Akiyama [17,18]. Equally, one can interpret these contour lines as being very similar to the shape of flow observed in the lab. Figure 4 shows the laboratory photo of caolinit-flow front [19] with the same inlet conditions, which is presented in Figure 3. Although some vortices are seen at the interface of the front of the experiment, the type of shape, especially the nose and location of the maximum depth of the two figures, are the same. In Figure 5, the averaged-layer depth of the turbidity current is compared with the experimental data [16]. In the numerical solution, the averaged-layer depth is calculated by the following expressions [12]:

$$u_{a\nu}(x)^2 h(x) = \int_0^\infty u(x,y)^2 dy, \tag{9}$$

$$c_{a\nu}(x) h(x) = \int_0^\infty c(x,y) dy, \tag{10}$$

$$Ri(x) = \frac{g'(x) h(x) \cos\theta}{u_{a\nu}(x)^2}, \tag{11}$$

$$g'(x) = g c_{a\nu}(x)(\rho_s - \rho_w)/\rho_w. \tag{12}$$

It can be seen from Figure 5, that present numerical results agree well with the experiments of Rad et al. [19]. The distribution of the horizontal velocity and concentration for $t = 500$ sec, at different axial locations, are shown in Figure 6. This figure should be studied in conjunction with Figure 3. Since the flow front lies under $x < 6$ m, thus, as seen from Figure 6a, the concentration at $x = 6$ m is zero. However, at the same point, velocity distributions, due to momentum diffusion, can be clearly observed in Figure 6b. Concentration and velocity distributions at $x = 2$ m indicate that the turbidity current has put the upper lighter fluid into movement. Due to the motion of two different layers of fluid, a kind of shear flow is established at the interface which is responsible for the production of vortices and, as a result, for the entrainment of the clear water into the turbidity current at the interface. The study of the variation of the concentration at $x = 2$ m, reveals that there is an abrupt increase in concentration near the solid boundary and the concentration is 30% higher than the input value. This increase is due to the settling of particles. The shoot-out seen in the curve at the bed, is a sign of particle sedimentation in that region. The distribution of the velocity and concentration with different sizes of particle, at $x = 1.36$ m, is plotted in Figure 7. The effect of the particle-size on the maximum velocity is small, as indicated in Figure 7a. However, this effect on the distribution of the concentration, is remarkably noticeable. For small-grain particles of less than 10-micron, the variation of

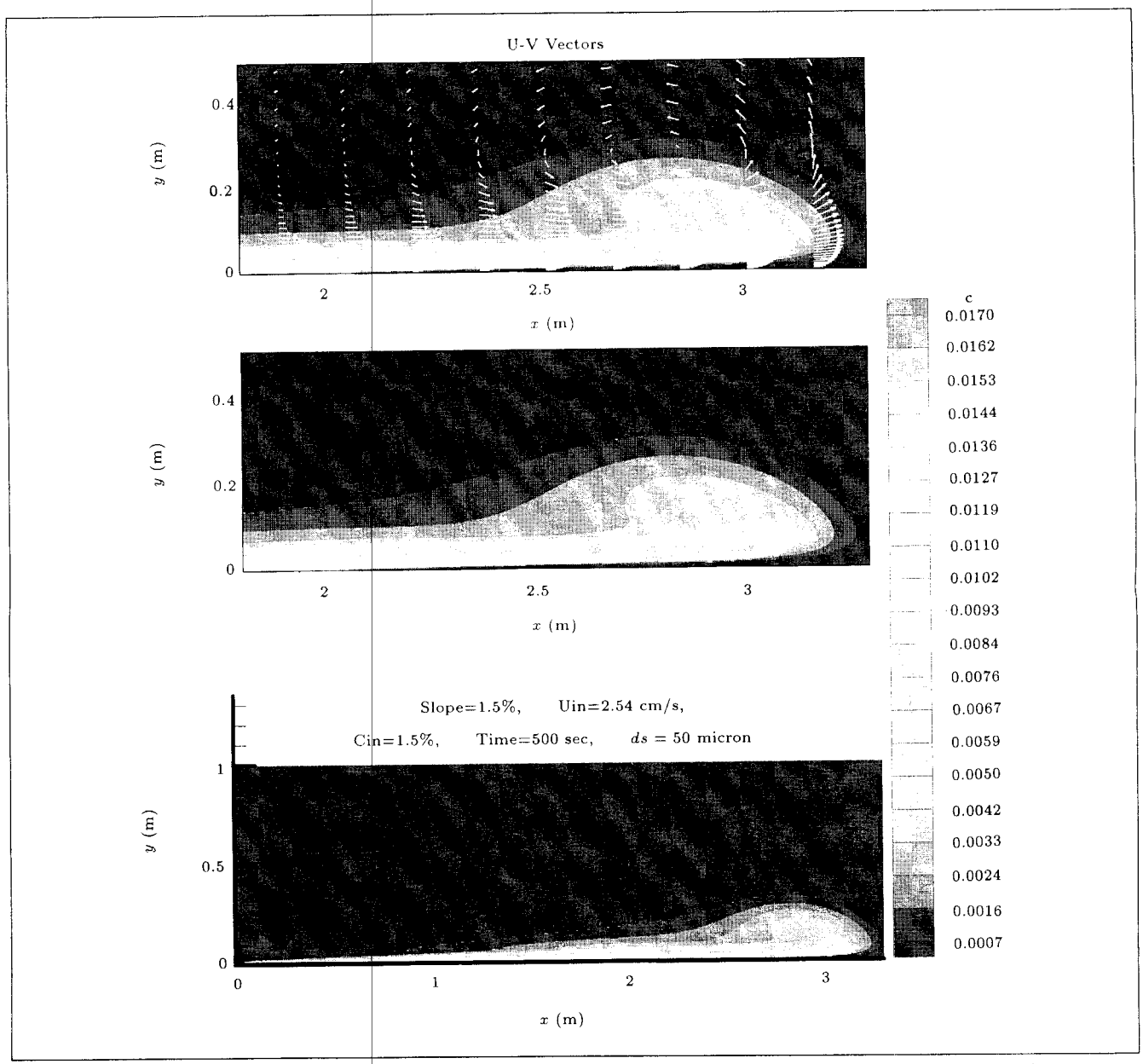

Figure 3. The contour lines of concentration and velocity vectors of the body and head of turbidity current after 500 sec from inlet, $\mathrm{Re}_i = 500$, $\mathrm{Ri}_i = 0.835$.

concentration is largely similar to the salt-water density current. Therefore, it can be postulated that the small-grain particles move with the same velocity as the fluid. Thus, the deposition of fine particles of less than 10 microns may take up to several months. This is one of the difficulties in desedimentation and percolation of rainwater to an underground supply. Particles of around 50 microns gradually deposit and increase the concentration of the particles near the bed up to 15 percent. At a further distance away from the bed, these particles can also preserve their concentration gradient and, therefore, contribute to advection. The study of concentration distribution for particles larger than 300 microns indicates a rapid fall-out and accumulation on the bed. Since the concentration of coarse sediment (sand) goes to zero at $y = 5.0$ cm above the bed, the fine particles (silt) will eventually diffuse further up to about $y = 7.0$ cm. It is noteworthy that for large-sized particle turbidity current, after settling, the low concentration flow continues moving, similar to a salt-water density current [20]. In this way, heavy floods containing large particles, are deposited rapidly, causing the floods to lose part of their driving force. As mentioned before, the settling velocity of particles in these computations were assumed to be constant. However, the settling velocity of particles depends on numerous factors such as neighborhood effects, concentration gradient, cohesive or non-cohesive material,

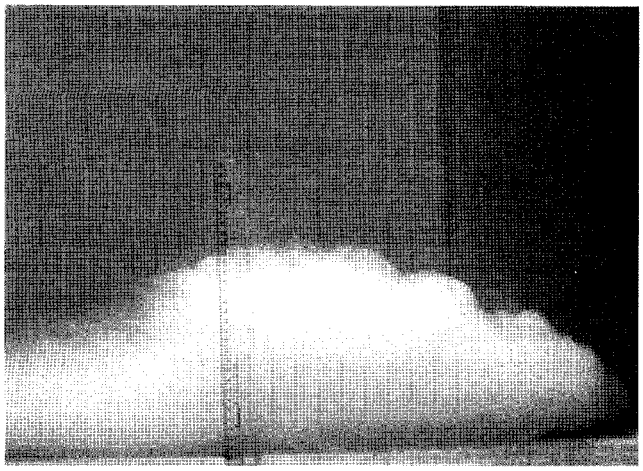

Figure 4. The laboratory photo of caolinit-flow front at the same inlet conditions of Figure 3.

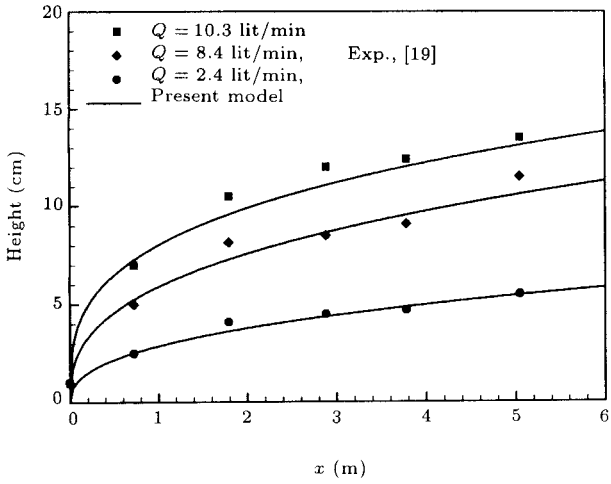

Figure 5. Comparison of averaged-layer depth with experimental data [19].

shape and level of turbulence and vortices present in the flow, particle shapes and sizes, etc. Up to now, no relation has been provided to account for, even empirically, the simultaneous effects of all these parameters.

Due to the entrainment of upper lighter fluid and turbidity current at the interface, the averaged-layer depth of the current, h, increases with x and, hence, the average velocity and concentration decrease. To calculate the entrainment rate, the Celik and Rodi [21] idea of conservation of particle mass was employed. The total rate of suspended sediment is:

$$q(x) = \int_0^\infty CUdy. \tag{13}$$

Here, the efficiency (the total of removal and entrainment) is defined as:

$$eff(x) = q(1) - q(x)/q(1). \tag{14}$$

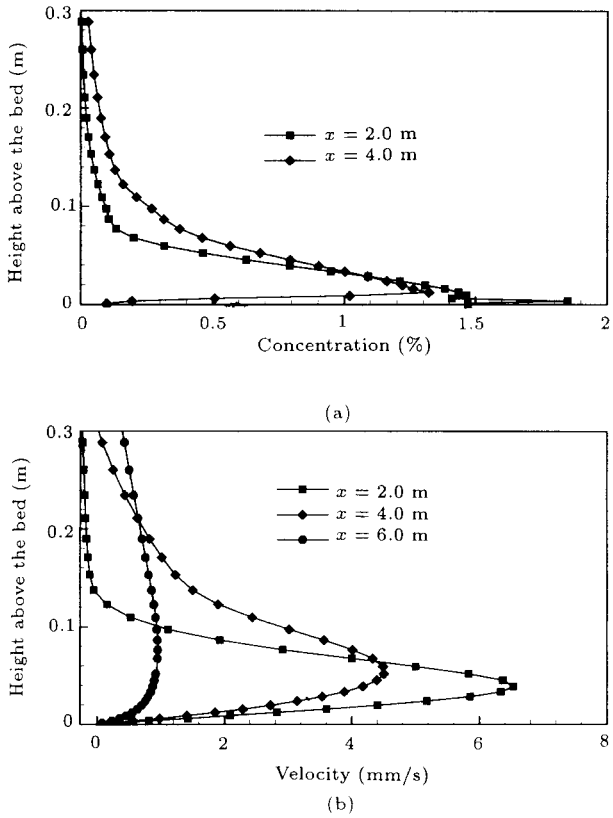

Figure 6. Velocity and concentration distribution in different locations of Figure 3.

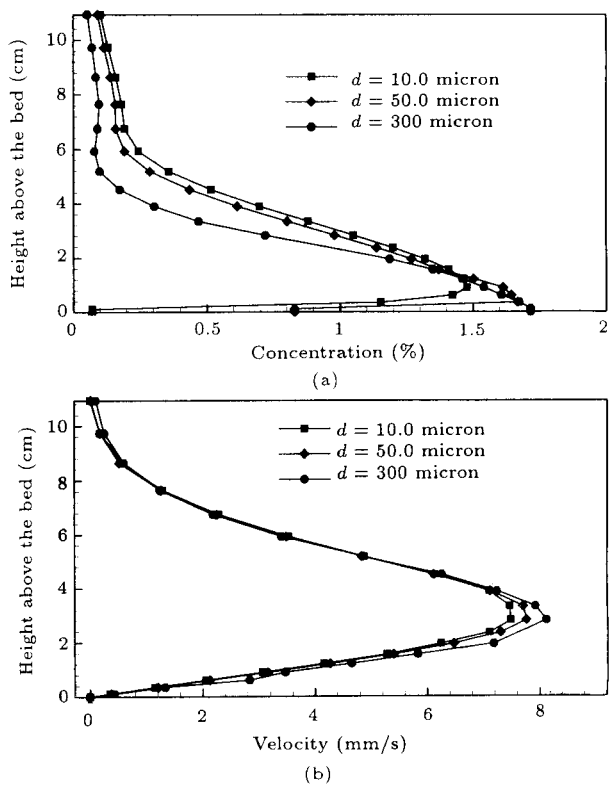

Figure 7. The effect of particle size on the distribution of concentration and velocity.

Figure 8 shows the effects of sizes of particles on efficiency. It can be seen that the $eff(x)$ decreased when the particles became large. Maximum $eff(x)$ is observed when there is no particle (salt-water solution) in the flow. This curve is the net entrainment rate. Figure 8 also shows that $eff(x)$ is always negative in a salt-water density current because of the entrainment of clear water. Due to the deposition of particles, $eff(x)$ of particle laden flow is increased and the subtraction of these two situations present the net rate of the deposition of particles.

$$\text{deposition rate} = eff_{(\text{with particles})} - eff_{(\text{no particles})}. \tag{15}$$

Figure 9 presents the effects of particle size on the deposition rate of turbidity currents. The input data of this calculation is from Rad [22]. It can be seen that when the size of particle increases, the deposition rate grows rapidly. In this manner, the bed-height of the deposition caused by turbidity currents was calculated. The bed-height is defined as:

$$bh(x) = T/(xl^{*}\rho_{dep})^{*}(\text{deposition rate}^{*}100), \tag{16}$$

where T is the siltation time of the turbidity current, ρ_{dep} is the density of wet deposition, and xl is the channel length. Figure 10 shows the comparison between the measured and computed bed-height of the deposition caused by turbidity currents. As can be seen, the computation values are in good agreement with the experimental data.

In this work, the effects of the simultaneous presence of two different particle sizes are also studied. Therefore, two equations of concentration (i.e., Equations 7 and 8) are simultaneously solved with the momentum and continuity Equations 1 to 3. This solution ignores the interaction of particles and, since the flow is laminar and concentration is low, this assumption is not far from reality. In this sample solution, it is assumed that 30% of the incoming fluid contains particles of about 50 microns and the rest contains small particles of about 10 microns. Figure 11 shows the velocity and concentration profiles of the turbidity current composed of two-grain sizes with different settling velocities. Since the flow is mainly made up of fine particles, they determine the overall distribution of concentration. As the coarse particles settle down near the bed, a locally reverse gradient is produced. The importance of reverse velocity and gradient is in the velocity profiles near the bed, as seen in Figure 11d. When the coarse particles gather along and near the bed, the normal velocity component, which often has a negligible magnitude in density currents compared to the horizontal component, becomes significant here

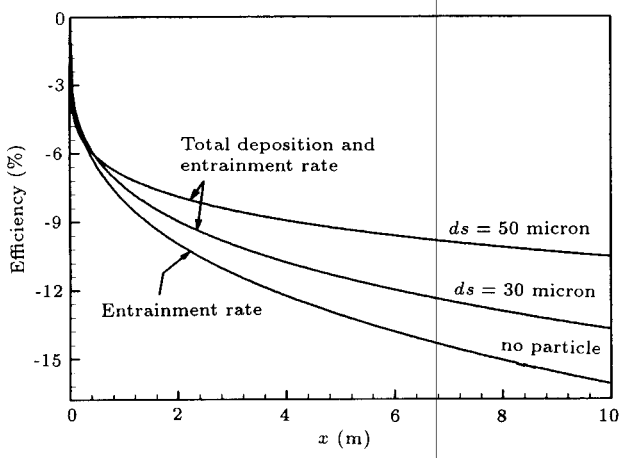

Figure 8. The efficiency of total entrainment and deposition rate of a turbidity current (Equation 14).

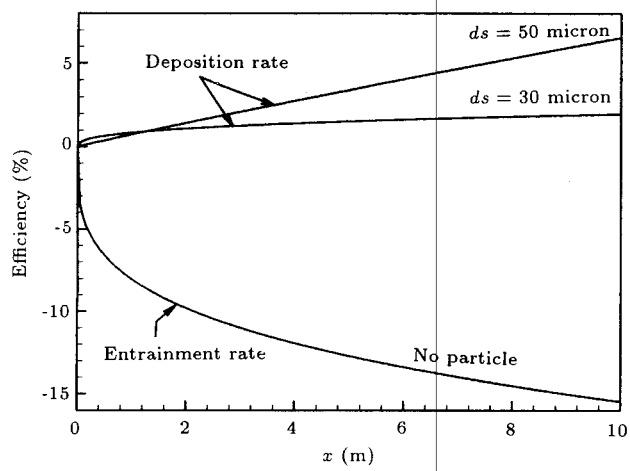

Figure 9. The deposition rate of turbidity current with different particle sizes.

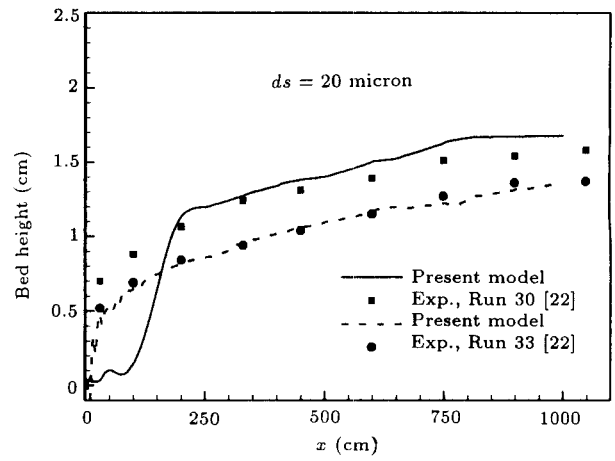

Figure 10. Comparison of bed height of deposition with experimental data.

and gives rise to small eddies near the bed. It is for the same reason (which was observed also in the lab) that the medium-sized particles do not deposit quickly. These particles, which settle down and deposit near the bed, perform a sliding and rolling motion and, thereby, create a kind of spongy layer, which moves with fluid [22]. However, the effects and the boundary deformation are neglected in this work. Figure 11d also demonstrates that the velocity profiles near the bed have been changed, due to the presence of particles. This indicates that the momentum interaction of fluid and particles in this region is considerable. This fact is usually ignored in the solution of sedimentary pools, where the equations of momentum and diffusion are not solved simultaneously [21].

CONCLUSIONS

The equations of particle-laden density currents are solved for the first time by the SIMPLEC method. The solution can show the shape of the front part, its body part and the distribution of the concentration and velocity profiles of the current. The results are compared with the experiments and show good agreement. This method can also provide the location of aggregation and sedimentation of particles besides the interaction of the momentum of fluid and particles close to the bed. The present model shows the role of the settling velocity of particles, which has the most influence on the vertical profile of the concentration and velocity components. The entrainment of clear water at the interface decreased the average velocity and concentration in each section. Based on the definition of the rate of suspended sediment material, the entrainment and deposition rates are calculated. In this work, the bed-heights of the deposition are estimated and generally, a good agreement is obtained. The effects of two particle sizes in the current are also investigated. In this case, each particle size decreases in suspension at a rate which depends on the settling velocity. This method could be applied for real mud fluid, which contains several particle sizes.

Simultaneous solution of the equations of momentum and concentration shows that independent solving of these equations is not effective enough. It seems that if different factors in the settling velocity of particles are taken into account; more realistic solutions could be obtained.

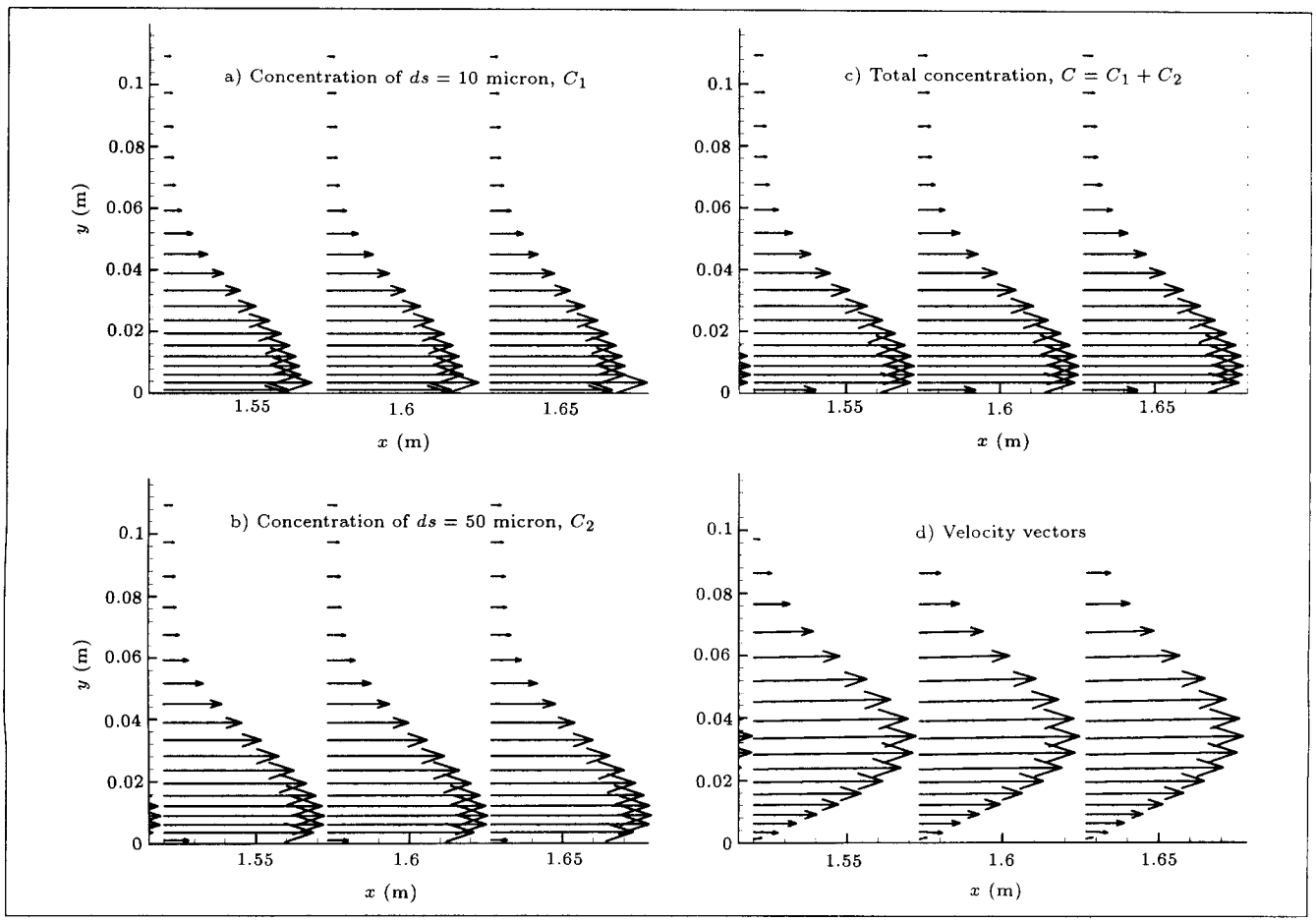

Figure 11. Presence of two sizes particles in the turbidity current.

NOMENCLATURE

b	height of sluice gate
C	concentration, $C = (\rho - \rho_w)/(\rho_s - \rho_w)$
ds	particles diameter
Fr	densimetric Froude number, Fr $= u/\sqrt{g'h\cos\theta}$
g	gravitational acceleration
g'	reduced gravitational acceleration $g' = g(\rho - \rho_w)/\rho_w$
h	density current depth
P	pressure
Re	Reynolds number, Re$= uh/\nu$
Ri	Richardson number, Ri$= g'h\cos\theta/u^2$
u	velocity in x direction
ν	velocity in y direction
ν_f	settling velocity of particles
u_{av}, c_{av}	cavaverage value of velocity and concentration
x	stream wise co-ordinate
y	transversal co-ordinate
λ	molecular diffusion
ρ	density of turbidity current
ρ_w	water density
ρ_s	particle density
θ	angle of the bed.

REFERENCES

1. Alavian, V. "Behavior of density current on an incline", *J. of Hydraulic Eng., ASCE*, **112**(1) (1986).
2. Simpson, J.E. "Gravity currents in the laboratory, atmosphere and ocean", *Ann. Rev. Fluid Mech.*, **14** (1982).
3. Alavian, V.G., Jiraka, H., Denton, R.A., Johnson, M.C. and Stefan, H.G. "Density current enters lakes and reservoirs", *J. of Hydraulic Eng., ASCE*, **118**(11) (1992).
4. Mukhamedov, A.M. "Origin and movement of bottom current in the reservoir of nurek power station and its effects on silting of the reservoir", *International Symposium on Stratified Flows*, Novosibrisk (1972).
5. Chikita, K. and Okumura, Y. "Dynamics of turbidity currents measured in katsurasawa reservoir, Hokkido, Japan", *J. of Hydrology*, **177** (1990).
6. Ford, D.E. and Johnson, M.C. "Field observation of density currents in impoundment", *Proc. Symp. On Surface Water Impoundment*, **2**, ASCE, New York, USA (1981).
7. Turner, J.S., *Buoyancy Effects in Fluids*, Cambridge University Press, London, UK (1973).
8. Benjamin, T.B. "Gravity currents and related phenomena", *J. Fluid Mech.*, **31** (1968).
9. Akiyama, J. and Stefan, H.G. "Turbidity currents with erosion and deposition", *J. of Hydraulic Eng., ASCE*, **111**(12) (1985).
10. Bonnecaze, R.T., Huppert, H.E. and Lister, J.R. "Particle driven gravity currents", *J. of Fluid Mech.*, **250** (1993).
11. Parker, G., Fukushima, Y. and Pantin, H.M. "Self-accelerating turbidity currents", *J. of Fluid Mech.*, **171** (1986).
12. Stacey, M.W. and Bowen, A.J. "The vertical structure of turbidity currents and a necessary conditions for self-maintenance", *J. Geophysical Research*, **93**(c4) (1988).
13. Lyn, D.A., Stamou, A.I. and Rodi, W. "Density currents and shear-induced flocculation in sedimentation tanks", *J. of Hydraulics Eng., ASCE*, **118**(6) (1992).
14. Fukushima, Y. "Numerical simulation of gravity current front", *J. of Hydraulic Eng. ASCE*, **124**(6) (1998).
15. Davidson, L. and Farhanieh, B. "A finite volume code employing collocated variable arrangement and cartesian velocity components for computation of fluid flow and heat transfer complex three-dimensional geometry", Chalmers University of Technology, Goteborg, Sweden (1991).
16. Farhanieh, B. and Sunden, B. "Laminar heat transfer and fluid flow in stream wise-periodic corrugated square ducts for compact heat exchangers", *HTD-V201, Compact Heat Exchangers for Power and Processes Industries*, Ed., Shah, R.K. et al. and ASME Book No. H00759 (1992).
17. Akiyama, J. and Stefan, H.G. "Turbidity current simulation in a diverging channel", *Water Resource Research*, **24**(4) (1988).
18. Akiyama, J., Ura, M. and Wang, W. "Physical-based numerical model of inclined starting plumes" *J. of Hydraulic Eng., ASCE*, **120**(10) (1994).
19. Rad, M. and Firoozabadi, B. "Confined turbidity current and its application in reservoirs", *Int. Conf. Civil Eng.*, Sharif University of Tech., Tehran Iran (1997).
20. Firoozabadi, B., Farhanieh, B. and Rad, M. "Numerical investigation of two-dimensional salt-water density current", *Fifth Conf. of Fluid Dynamics*, Ferdousi University, Mashhad, Iran (in Persian) (1998).
21. Celik, I. and Rodi, W. "Modeling of suspended sediment transport in non-equilibrium situations", *J. of Hydraulic Eng., ASCE*, **114**(10) (1988).
22. Rad, M. "The deposition of silt in reservoirs by density currents", Ph.D. Thesis, Imperial Coll., London University, UK (1976).